ADVANCED FUNCTIONAL MATERIALS
www.afm-journal.de



# Significantly Enhanced Thermoelectric Performance in n-type Heterogeneous BiAgSeS Composites

*Di Wu, Yanling Pei, Zhe Wang, Haijun Wu, Li Huang, Li-Dong Zhao,* and Jiaqing He**

**High performance n-type bulk BiAgSeS is successfully synthesized to construct heterogeneous composites which consist of mesoscale grains of both pristine BiAgSeS and doped $BiAgSeS_{1-x}Cl_x$ ($x = 0.03$ or 0.05). Without perceptibly deteriorating the Seebeck coefficient, a significant enhancement on electrical conductivity is obtained due to an anomalous increase of both carrier mobility and concentration; the enhanced carrier mobility is proven to be a direct result of modulation doping which relates to the band alignments, while the increased carrier concentration is attributed to the possible charge transfer from Cl rich nanoscale precipitates at the heterogeneous BiAgSeS/$BiAgSeS_{1-x}Cl_x$ grain boundaries. Eventually, an enhanced figure of merit $ZT \approx 1.23$ at 773 K in the composite $(BiAgSeS)_{0.5}(BiAgSeS_{0.97}Cl_{0.03})_{0.5}$ is achieved, indicating that heterogeneous composites ultilizing the mechanism of modulation doping shall be a promising means of boosting the performance of thermoelectric materials. This strategy should be very likely applicable to other thermoelectrics.**

## 1. Introduction

Thermoelectric materials can harvest electricity directly from waste heat, thus have drawn growing research interests for decades. The performance of a thermoelectric material is determined by a dimensionless figure of merit $ZT = S^2\sigma T/\kappa$, where $S$ is the Seebeck coefficient, $\sigma$ is the electrical conductivity, $T$ is the absolute temperature in Kelvin and $\kappa$ is the thermal conductivity. Although these transport parameters are interdependent, the enhancement of $ZT$ can generally be obtained via improving the power factor $S^2\sigma$ and reducing the thermal conductivity $\kappa$. Strategies aiming at improving the power factor via the Seebeck coefficient $S$, such as resonant states,[1,2] band convergence,[3,4] energy filtering/thermoionic emission[5,6] and recent phase transition,[7,8] were meticulously studied in theory and also experimentally realized. Besides, during the past decade, tremendous efforts have also been devoted to reduce the thermal conductivity by various nanostructuring techniques.[9–13] Meanwhile, seeking for materials with intrinsically low thermal conductivities, for example, partially filled skutterudites[14] and clathrates with caged frameworks,[15] Zintl phases with complex crystal structures,[16] metal oxides with layered structures,[17–19] materials with unbound lone-pair valence electrons,[20,21] and huge anharmonicity,[22] are also persistently igniting researchers' enthusiasms. However, a bottle neck was faced, when the intrinsical thermal conductivities for these materials approached the corresponding glass limits.[20] Therefore, improving the electrical transport performance, namely, the power factor, seems to be one and the only feasible strategy to further lift up $ZT$ for these thermoelectrics.

Recenlty, BiAgSeS was reported a promising n-type thermelectric material with intrinsically low thermal conductivity of 0.29 W $m^{-1}$ $K^{-1}$ at 823 K due to natural nanoscale precipitates and lone-pair electrons of Bi.[23] Although the electrical transport properties of BiAgSeS were enhanced through $Cl^-$ doping in the $S^{2-}$ site, the electrical conductivity of $BiAgSeS_{1-x}Cl_x$ is still low (≈160 S $cm^{-1}$) even with the maximal doping level $x = 0.05$, compared with those of state-of-the-art thermoelectrics (>1000 S $cm^{-1}$),[24–26] thus leaving room for further improvement. Moreover, monotonically increasing the carrier concentration can greatly deteriorate the Seebeck coefficient, as the well-known Pisarenko relation indicates, therefore might result in an overall inferior thermoelectric power factor.

Modulation doping[27,28] (MD) is a well-developed technique widely used in thin-film devices in order to improve the electrical conductivity. A typical device utilizing the notion of modulation doping consists of three active layers,[29] that is, a doped layer which provides charge carriers, an undoped layer which serves as charge transport channel free of parent impurity atoms and a thin spacer layer which spatially separates the above two layers. The doped layer normally has a higher/lower conduction/valence band edge than the undoped one for n/p-type doping, so as to make it feasible that electrons/holes can be spilled into the undoped layer where much less impurity scattering is present. The spacer layer is essential[30] from the perspective of preventing impurity diffusion from the doped layer to the undoped channel, otherwise, the effect of modulation doping would be attenuated. For several decades, the application of modulation doping has been limited to the thin-films for charge carrier

Dr. D. Wu, Z. Wang, H. J. Wu, Dr. L. Huang,
Prof. J. Q. He
Department of Physics
South University of Science and Technology of China
Shenzhen 518055, P. R. China
E-mail: he.jq@sustc.edu.cn
Dr. Y. L. Pei, Dr. L.-D. Zhao
School of Materials Science and Engineering
Beihang University
Beijing 100191, China
E-mail: zhaolidong@buaa.edu.cn

DOI: 10.1002/adfm.201402211

transport along the film plane, while that in three-dimensional bulk remains unexplored. Recently, Zebarjadi et al.[31] and Yu et al.[32] reported that the power factor of $Si_{1-x}Ge_x$ series could be significantly enhanced via constructing a heterogeneous composite by mechanically mixing two types (doped and undoped) of $Si_{1-x}Ge_x$ nanograins (with different $x$). The carrier mobility as well as the overall power factor were found to be significantly enhanced, and the underlying mechanism was attributed to modulation doping, as in the two-dimensional thin-films, i.e., charge carriers spill over from the doped grain to the undoped grains due to the specific band offset between them. Some other heterogeneous structures reported by Zhao et al.[33] and Koirala et al.[34] also exhibit improved power factors, utilizing metal nanoparticles instead of doped grains to provide charge carriers to undoped semiconductor matrix; nevertheless, in their cases, the enhanced power factor might come completely from carrier concentration optimizing, since direct evidence of carrier mobility enhancement was provided in neither of these works.

In this work, we construct heterogeneous BiAgSeS composites by incorporating pristine BiAgSeS grains with a certain volume fraction of $BiAgSeS_{1-x}Cl_x$ ($x$ = 0.03 or 0.05) grains, and achieve improved power factor via simultaneouly increasing the carrier mobility and concentration in the notion of modulation doping (MD). Thereby, we achieved a significantly enhanced power factor (87% higher than uniformly doped (UD) sample with the same nominal composition at 823 K). Without severely deteriorating the thermal conductivity, an outstanding thermoelectric figure of merit ZT~1.23 was obtained at ≈773 K for the MD composite $(BiAgSeS)_{0.5}(BiAgSeS_{0.97}Cl_{0.03})_{0.5}$, which is 22% higher than that of the uniformly doped $BiAgSeS_{0.97}Cl_{0.03}$ ($ZT \approx$ 1.0 at 823 K) with optimized carrier concentration.[23]

## 2. Results and Discussions

A heterogeneous composite $(BiAgSeS)_{0.7}(BiAgSeS_{0.95}Cl_{0.05})_{0.3}$ (MD_A in what follows) was synthesized following the method described in the experimental section, by mixing mesoscale grains of pristine BiAgSeS and $BiAgSeS_{0.95}Cl_{0.05}$ at a volume ratio of 7:3. BiAgSeS owns a rock-salt based structure, **Figure 1**a. The heterogeneous sample MD_A is identified to be of single rock-salt phase by powder X-Ray Diffraction (XRD) pattern, Figure 1b; no impurity phases were discovered upon the processes of mechanical mixing and high temperature consolidating. Keeping the nominal composition unmodified, we synthesized another heterogeneous composite $(BiAgSeS)_{0.5}(BiAgSeS_{0.97}Cl_{0.03})_{0.5}$ (MD_B) following the similar procedures of MD_A, to investigate the effect of a different volume fraction of pristine region (with higher carrier mobility) on the overall electrical properties and to further evidence the generality of the efficacy of modulation doping in enhancing TE performance. The thermoelectric properties of the two modulation doped samples are compared with those of their parent components, Figure S1–S4 (Supporting Information).

We observed a consistent outperformance of modulation doped composites over their parent components, which strongly indicates new mechanism(s). Bergman[35] has once proven that the $ZT$ value of a composite cannot exceed the largest value of its parent components, without considering the influence of interface effect or charge transfer, although some later works[36] proved it wasn't absolutely correct in some rigorous cases. In our modulation doped samples, the typical grain size is ≈500 nm, as shown in the transmission electron microscopy (TEM) images later. The relatively low density of boundaries of such large-size grains is believed to be fairly ineffective in scattering phonons, not to mention scattering charge carriers, since the mean free path of electrons is only around 1–2 nm.[37] Thereby, it is highly possible that the outperformances of MD_A and MD_B over their parent materials originate from the charge transfer between doped and undoped grains in the notion of modulation doping.

The advantages of modulation doping over uniformly doping can be well illustrated via comparing the thermoelectric properties of the modulation doped samples directly with their uniformly doped counterpart $BiAgSeS_{0.985}Cl_{0.015}$. As seen in **Figure 2**a,b, at room temperature, although the absolute values of the Seebeck coefficient are reduced from 343 μV/K for uniformly doped $BiAgSeS_{0.985}Cl_{0.015}$ to 311 μV/K for MD_A and 300 μV/K for MD_B, the enhancements on the electrical conductivity of modulation doped samples can overcompensate the loss on the Seebeck coefficients. This phenomenon of overcompenzation lasts throughout the whole temperature range of measurements. As a result, the power factor is lifted up by 78% for MD_A and 87% for MD_B, respectively, from uniformly doped $BiAgSeS_{0.985}Cl_{0.015}$, Figure 2c. The almost identical lattice thermal conductivity of all compositions implies that modulation doping doesn't provide any extra effective phonon scattering mechanisms, see Figure 2e. For uniformly doped $BiAgSeS_{0.985}Cl_{0.015}$, the maximal $ZT \approx 0.74$ is achieved at 823 K; upon modulation doping, Figure 2f, this value is improved by 49% to ≈1.10 at 773 K for sample MD_A and by 67% to ≈1.23 at 773 K for sample MD_B, implying that the application of modulation doping in bulk BiAgSeS by simply incorporating two different types of grains can indeed lead to significant enhancements on thermoelectric performance, without changing the nominal composition. The application of this technique to other bulk thermoelectrics is also highly plausible.

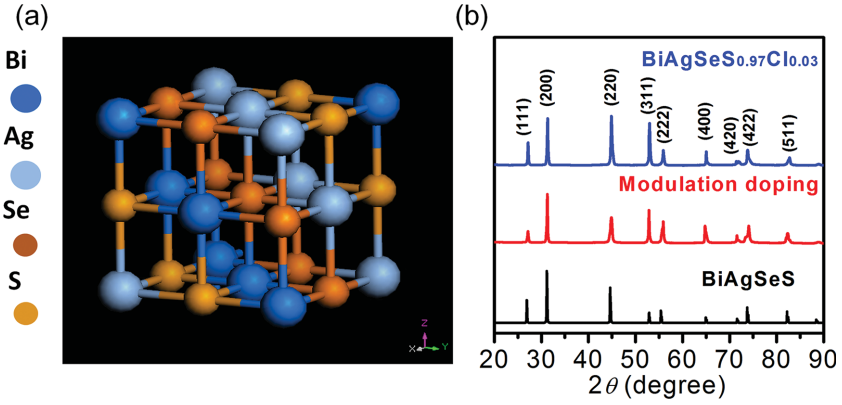


**Figure 1.** a) Schematic rock-salt crystal structure of BiAgSeS, b) powder XRD patterns showing pure cubic phase in the modulation doped $(BiAgSeS)_{0.7}(BiAgSeS_{0.97}Cl_{0.05})_{0.3}$ sample.

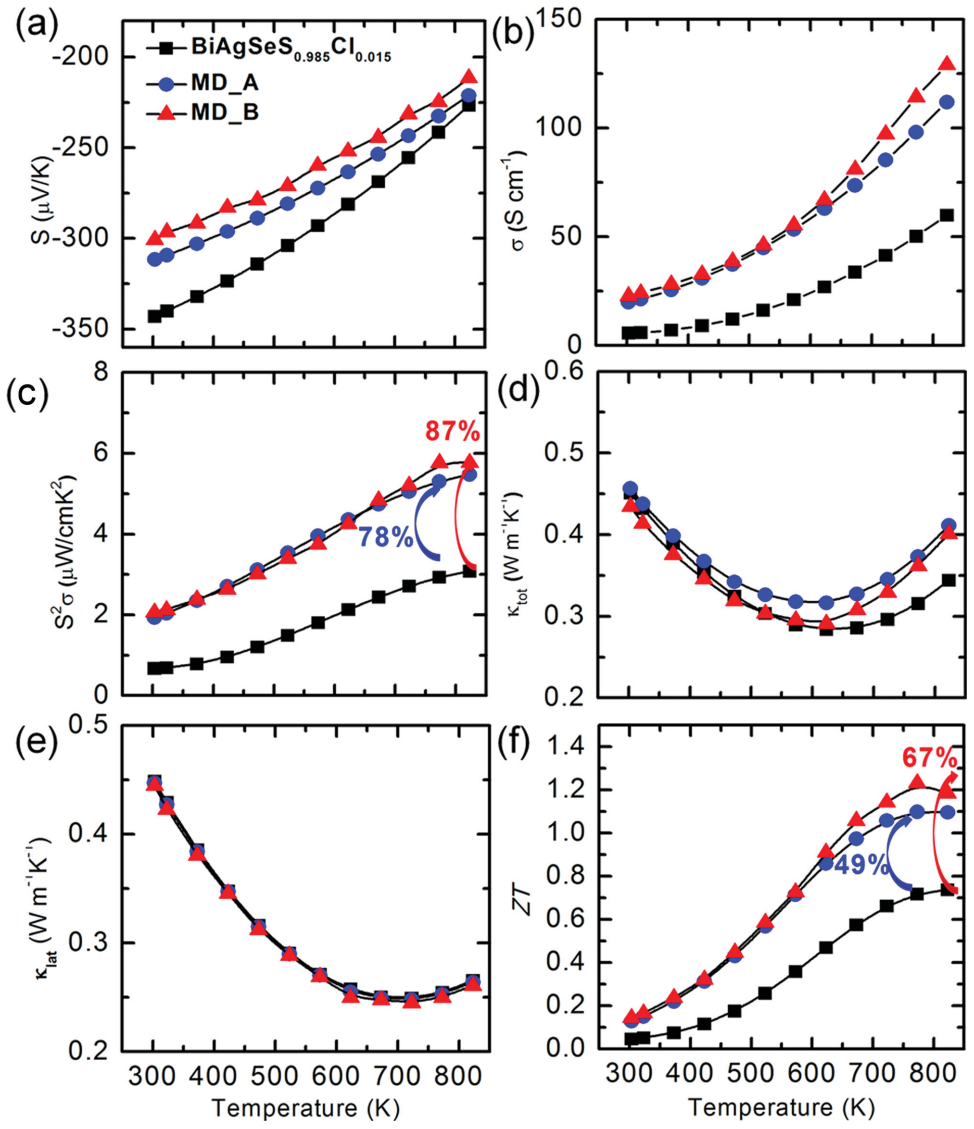


**Figure 2.** The comparison of the a) Seebeck coefficient, b) electrical conductivity, c) power factor, d) total thermal conductivity, e) lattice thermal conductivity, and f) figure of merit *ZT* between $(BiAgSeS)_{0.7}(BiAgSeS_{0.95}Cl_{0.05})_{0.3}$ and $(BiAgSeS)_{0.5}(BiAgSeS_{0.97}Cl_{0.03})_{0.5}$ and the uniformly doped counterpart $BiAgSeSCl_{0.015}$. The power factor is increased by 78% and 87%, corresponding figure of merit *ZT* is increased by 49% and 67% from uniformly doped sample to MD_A and MD_B, individually.

As mentioned earlier, the enhanced thermoelectric performance in previous works of Zhao et al.[33] and Koirala et al.[34] might largely come from the carrier concentration tuning, while the heterogeneous $Si_{1-x}Ge_x$ composites reported by Zebarjadi et al.[31] and Yu et al.[32] did provide solid evidence that the carrier mobility was indeed improved upon modulation doping, with the carrier concentration almost unchanged. Hall mobility data is thus essential to clarify whether the underlying mechanism for the enhanced electrical conductivity can be solely ascribed to modulation doping or not. Rather surprisingly in our case, besides the enhanced carrier mobility, it is found that the carrier concentration is also increased in our modulation doped samples, compared with the uniformly doped counterpart,[23] as seen in **Figure 3**. For sample MD_A, the carrier concentration $n$ is promoted from $\approx 3 \times 10^{18}$ cm$^{-3}$ for the uniformly doped $BiAgSeS_{0.985}Cl_{0.015}$ to $\approx 7 \times 10^{18}$ cm$^{-3}$, meanwhile, the carrier mobility $\mu$ increases simultaneously from $\approx$12.5 cm$^2$/Vs to $\approx$15.5 cm$^2$/Vs; for MD_B, $n$ is promoted to $\approx 1.0 \times 10^{19}$ cm$^{-3}$, and $\mu$ increases to $\approx$14.0 cm$^2$/Vs. Our initial motivation of applying modulation doping is merely to improve the electrical conductivity via boosting the carrier mobility, and this is indeed sufficiently supported by the measured Hall mobilities; nevertheless, there must exist some other unknown mechanism which shall be responsible for the increased carrier concentration observed in the MD systems.

In order to explore the underlying mechanisms of synergistically enhanced carrier mobilities and concentrations in MD samples, we carried out a systematic investigation on the microstructures of both uniformly doped and modulation doped samples using various TEM techniques. Large-scale precipitates are always found in mesoscale grains for uniformly doped $BiAgSeS_{1-x}Cl_x$ ($x = 0.03$), as shown in **Figure 4** and S5. Energy dispersive spectrometer (EDS) line scanning (inset in Figure 4b)

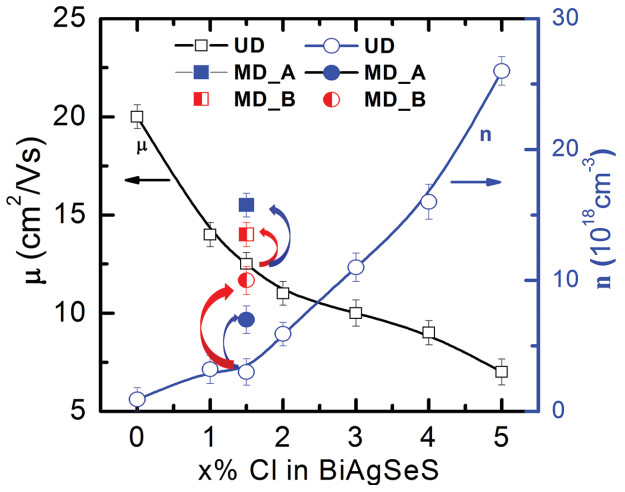


**Figure 3.** A simultaneous enhancement on carrier concentration and carrier mobility is found on both modulation doped samples MD_A and MD_B. (UD presents the uniformly doped sample $BiAgSeS_{0.985}Cl_{0.015}$).

reveals that these large-scale precipitates (20–50 nm) are Cl rich, and mostly segregated in the matrix grains. The location of these Cl rich precipitates in the uniformly doped sample is very different from that of precipitates in MD samples, as shall be seen later. The widespread precipitation of Cl can also be understood by the relatively low solubility of Cl in BiAgSeS, since a 1 atm% complete substitution of S by Cl would result in ≈1.06 × $10^{20}$ $cm^{-3}$ electron concentration (≈1% × $N_A\rho/M$, $N_A$-Avogadro constant, $\rho$-mass density, $M$-molecular mass), which is much larger than the actual Hall concentration of ≈1.1 × $10^{19}$ $cm^{-3}$ in $BiAgSeS_{0.97}Cl_{0.03}$. The laminated precipitates ($BiAgSe_2$), all located in the matrix grains of pristine BiAgSeS in our previous work,[23] were not seen in uniformly doped $BiAgSeS_{1-x}Cl_x$, thus it seems that the formation of those laminated precipitates was suppressed through Cl doping. The grain boundaries are also always arrayed with dislocations to relieve the strain between misaligned grains, as shown in Figure 4c,d.

Low-magnification images in **Figure 5**a of modulation doped sample MD_B show mesoscale grains with an average size of ~500 nm. Those four enlarged images in the bottom row of

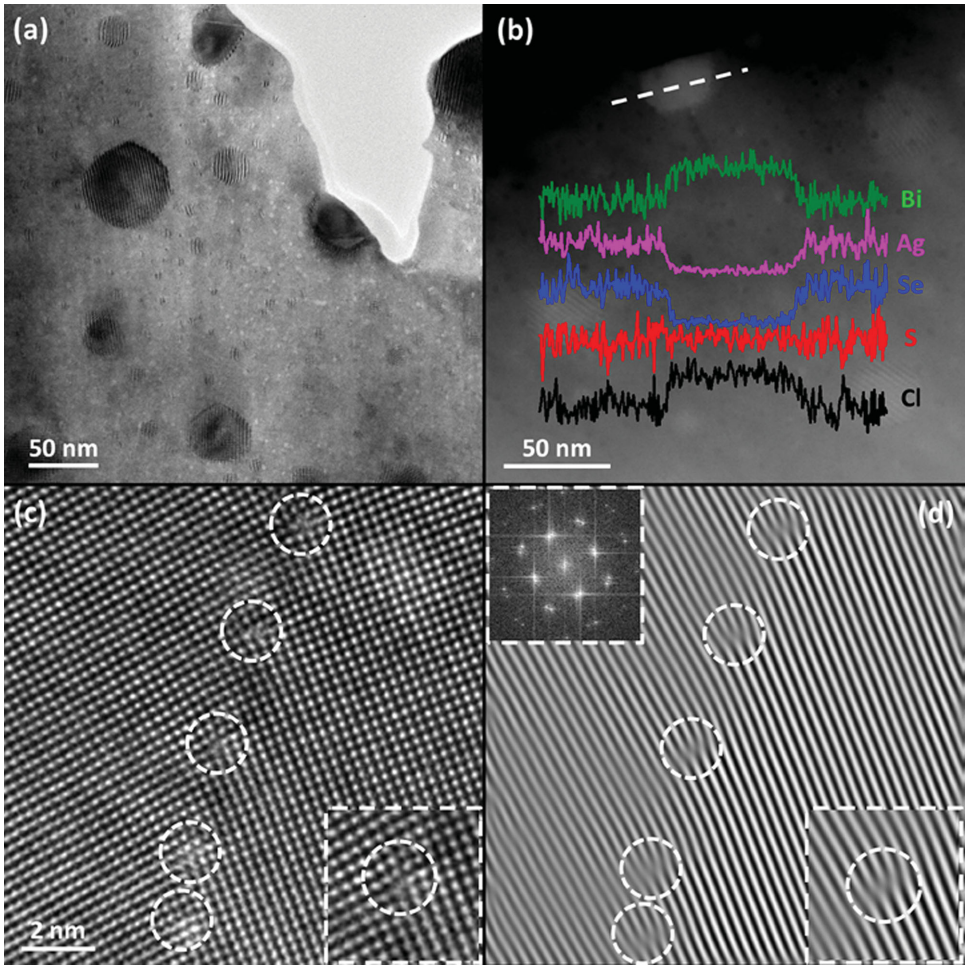


**Figure 4.** a) Medium-magnification image of $BiAgSeS_{0.97}Cl_{0.03}$ sample shows large-scale precipitates and nanoscale precipitates inside one grain. b) Medium-magnification HAADF image with inserted EDS line scanning show Bi and Cl rich feature of large-scale precipitates. c) High-magnification image shows a grain boundary with arrayed dislocations along [001] zone axis. d) IFFT image of (c). The inset FFT image from boundary shows peak splitting.

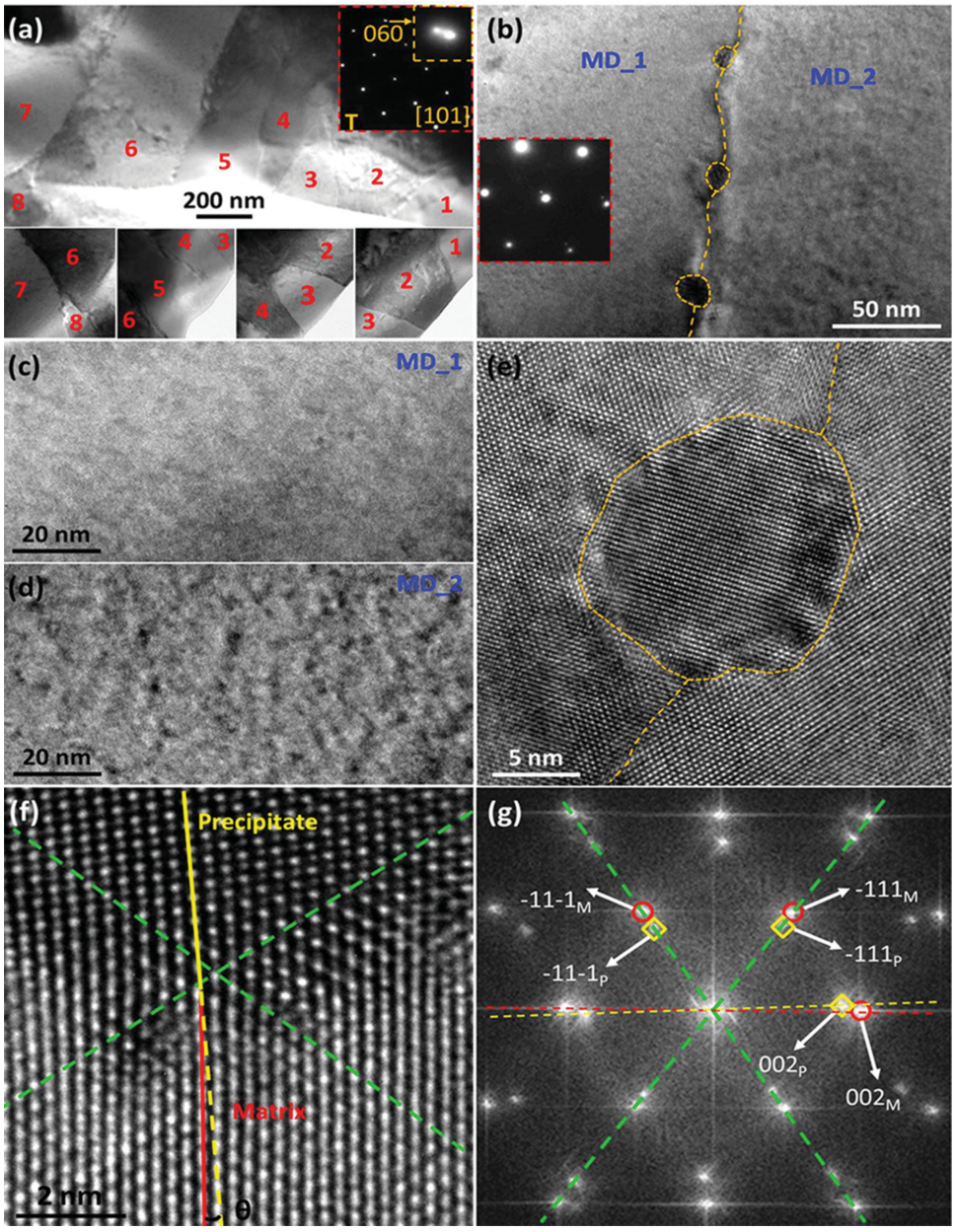


**Figure 5.** a) Low-magnification images of sample MD_B show mesoscale grains. The inset SAED pattern in the upper image shows small-angle peak splitting. b) Medium-magnification TEM image shows two distinct regions with a precipitate-linking boundary. The weak spots beside the main spots in the inset SAED pattern are from the precipitates. c) Medium-magnification TEM image from MD_1 region shows roughly homogeneous contrast with very little precipitates, indicating smaller Cl fraction. d) Medium-magnification TEM image from MD_2 region shows nanoscale precipitates, indicationg higher Cl fraction. e) High-magnification TEM image shows one large precipitate on the boundary, boundary is marked with yellow dashed line. f,g) Lattice and IFFT image show the crystallographic relation between precipitate and matrix at the precipitate-matrix interface. Dashed green lines show sharing planes between precipitate and matrix, while red and yellow lines show the inconsistent planes of precipitate and matrix.

Figure 5a were obtained when one of the grains was tilted to zone axis, so that the grain boundaries can be observed clearly. The peak splitting in the inserted electron diffraction pattern can only be seen at high order reflections, indicating the crystallographic misorientation between neighboring grains is small. Figure 5b and Figure S6a are medium-magnification TEM images of a typical grain boundary, showing two distinct MD grains (marked as MD_1 and MD_2) with a precipitate-linking boundary. These precipitates are also rich of Cl element, as in uniformly doped sample. The weak spots beside the main ones in the inset electron diffraction pattern are from the precipitates. To explicitly disclose the difference between MD_1 and MD_2, Figure 5c,d, and Figure S6b,c are then selected based on the similar thickness under the same magnification. MD_1 grain exhibits roughly homogeneous contrast with almost no precipitates, indicating a smaller Cl doping fraction in BiAgSeS, Figure 5c and Figure S6b; while MD_2 grain in Figure 5d and Figure S6c shows a certain density of nanoscale (1–2 nm) precipitates, thus implying a higher Cl doping fraction

than the solid solubility of Cl in BiAgSeS. This distinction is a strong evidence of a heterogeneous structure. However, due to the low solubility of Cl in BiAgSeS, the actual atomic fraction of Cl in the matrix region is well below the resolution of EDS scanning, which makes it unlikely to provide direct evidence of the visible Cl content in MD_1 and MD_2 regions. Nevertheless, the distinct grain boundaries between MD samples and uniformly doped sample strongly imply that a compositional difference between the two sides of the grain boundary exisits in MD samples. It is indeed the existence of slight Cl doping difference between these adjacent modulated grains and the relatively less obstructed carrier transport in the low doping regions that lead to the overall enhanced carrier mobility. Note that the the absence of laminated precipitates in our MD samples (especially in region MD_1) might come from the inevitable diffusion of Cl from doped to undoped regions, which suppressed the formation of $BiAgSe_2$ precipitates.

Besides the modulated grains as discussed above, we also need to look through the grain boundaries between the heterogeneous MD_1 and MD_2 grains. Large-scale precipitates (around 20 nm in size) array exclusively on the boundary, which is thus called precipitate-linking boundary, Figure 5b, Figure S6a,d. The formation of these large-scale Cl-rich precipitates can be imagined as that the Cl dopants would diffuse from heavily doped regions to undoped regions, but some of them are blocked at the defects along the boundaries. A high-magnification TEM image in Figure 5e clearly shows such type of precipitates. The boundary around the precipitate is marked with yellow line in Figure 5e, which clearly reveals the crystalline relation between these precipitates and the boundary. Such a boundary is distinct from the traditional one which always possesses a sharp interface with a large misorientation between the two sides, instead, it exhibits a weak interface contrast, predicting an endotaxial relation between MD_1 and MD_2 grains. Along the precipitate-linking boundary of MD samples, there are two types of interfaces or boundaries: one between MD_1 and MD_2 grains, and the other between precipitates and the MD_1/MD_2 matrix. Figure 5f is a lattice image along [110] zone axis showing such precipitate-matrix interface. The Fast Fourier Transform (FFT) image of Figure 5g shows that the crystallographic relation between precipitate and matrix is also endotaxial. Both precipitate and matrix share (-111) and (-11-1) planes (marked with green dashed lines), but are inconsistent along (002) planes (marked with yellow and red dashed lines respectively) with a misorientation angle $\theta$ of 2°. The structure features of the precipitate-matrix interface of MD samples are quite similar with those in Cl uniformly doped samples ($x$ = 0.03), as shown in Figure 4a. It has been clearly shown that the endotaxial crystallographic features of both types of interfaces discussed above could facilitate carrier transport but cause phonon scattering, and thus play an important role in optimizing the electrical and thermal transport properties of thermoelectrics.[38] Furthermore, large-scale precipitates confined on the boundary between modulated grains not only release the strains between misaligned grains, but also could act as charge carriers (electrons in our case) reservoirs, providing additional electrons to the modulated grains when the whole material is applied under the external thermal or voltage gradient, which is possibly the origin of the increased carrier concentration found in our MD samples.

To disclose the exclusive contribution of modulation doping to the thermoelectric performance, one has to eliminate the disturbance coming from carrier concentration difference. Hereby, we present in **Figure 6** the dependence of

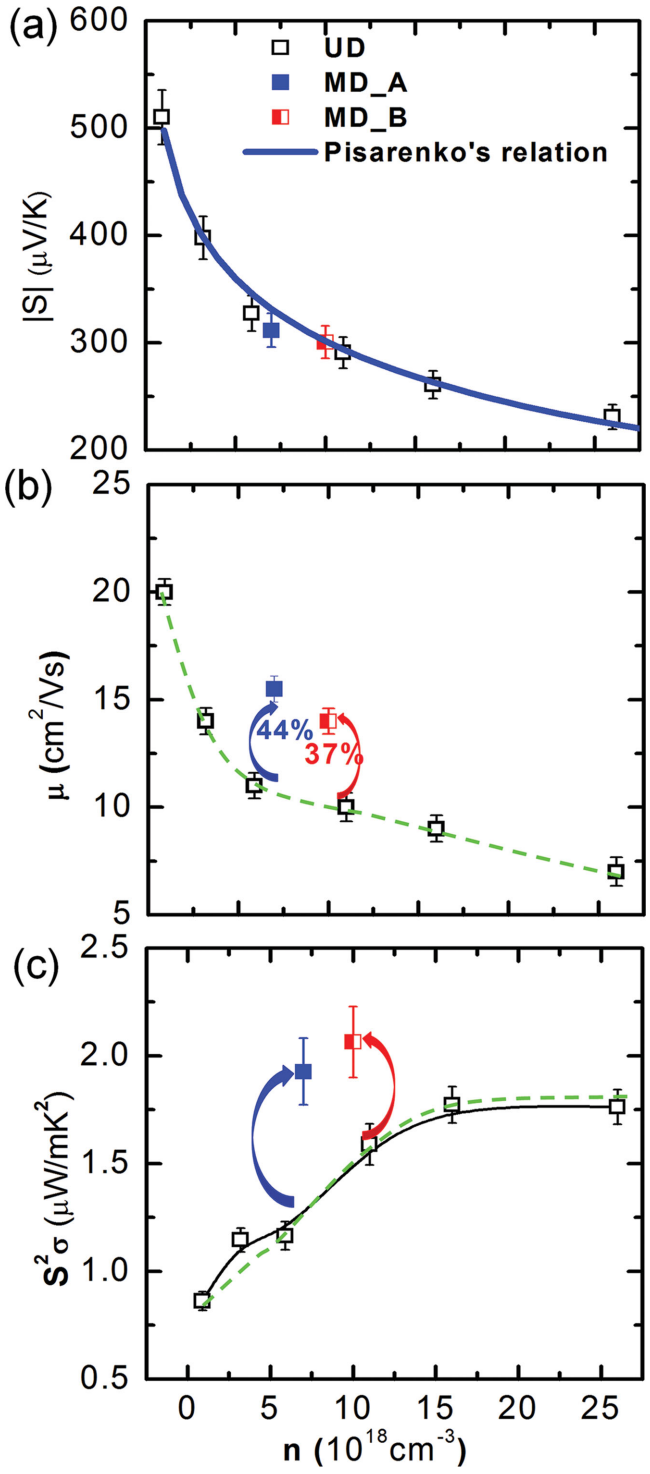


**Figure 6.** The dependence of the a) Seebeck coeffcient and b) carrier mobility on carrier concentration at room temperature indicates that the improvement on c) the power factor comes purely from the promotion of carrier mobility due to modulation doping, with the electronic structures and scattering mechanism of charge carriers almost unaltered. (UD presents the uniformly doped samples).

thermoelectric properties of MD and uniformly doped (UD) samples on carrier concentration, and the discussion is constrained to room temperature if not explicitly mentioned. The absolute values of the Seebeck coefficients of uniformly doped samples $BiAgSeS_{1-x}Cl_x$[23] ($x$ = 0, 0.01, 0.02, 0.03, 0.04 and 0.05) with corresponding carrier concentrations are plotted in Figure 6a. The inversely related $S$ and $n$ is consistent with the Pisarenko's relation (blue solid line, details in SI); the observation that the Seebeck coefficients of the two MD samples also locate close to the Pisarenko line suggests that modulation doping has no marked effects in perturbing the electronic density of states of BiAgSeS. The dependence of the carrier mobilities on carrier concentration is shown in Figure 6b. The open squares linked with a dash line illustrate that the carrier mobility of uniformly doped sample decreases as the carrier concentration (Cl doping level) increases. Dissimilar to the $S$ versus $n$ relation in Figure 6a, upon modulation doping, the carrier mobility $\mu$ is lifted up to a much higher plateau, specifically, $\mu$ is enhanced by ≈37% at $n = 1.0 \times 10^{19}$ cm$^{-3}$, and by ≈44% at $n = 7 \times 10^{18}$ cm$^{-3}$. It is unlikely to conclude that a higher volume fraction of charge transport channel (MD_A) causes a larger relative enhancement of $\mu$, due to the considerably small difference between the two percentages (44% for MD_A and 37% for MD_B). The enhancement of carrier mobility at the same carrier concentration is a direct result of charge transfer and redistribution between pristine and doped grains, in the notion of modulation doping. Combining the "normal" behavior of $S$ vs $n$ and "abnormal" $\mu$ versus $n$, the overall power factor $S^2\sigma$ is significantly enhanced at a fixed $n$, strongly validating a successful application of modulation doping in bulk BiAgSeS materials. It is interesting to find that Dehkordi et al.[39] also observed similar phenomenon as what we have. In their case, a charge carrier transport channel constructed of a grain boundary phase shall be responsible to the enhanced carrier mobility. Considering the relatively large volume fraction of the grain boundary phase, their strategy might also be taken as modulation doping to some extent.

The Density Function Theory (DFT) calculations (details in Supporting Information) are used to find out the conduction band offset $\Delta E_c$ (before contact) between pristine BiAgSeS and doped $BiAgSeS_{1-x}Cl_x$. Our calculation shows that the substitution of Cl on S site results in little change on the energy level of conduction band miminum (CBM), that is, a $x \approx 6.25\%$ (1/16) Cl doping level lifts the CBM up by only 30 meV. On the other hand, a 1% absolute substitution of S by Cl would bring about ≈$1.06 \times 10^{20}$ cm$^{-3}$ electron concentration, indicating the effective doping levels ($x$ values) of Cl for $BiAgSeS_{0.97}Cl_{0.03}$ and $BiAgSeS_{0.95}Cl_{0.05}$ are only ≈0.104% and ≈0.245%, respectively. It can thus be expected that such a small fraction of Cl substituting S would lead to negligible CBM shifting. In our following calculations, it ought to be accurate enough for us to take the band offset $\Delta E_c$ between pristine and doped components as 0, and the band alignment is then schematically plotted as in Figure S7a (Supporting Information).

We estimate the carrier redistribution in the two distinct grains with a model discussed in the Supporting Information , and then adopt a self-consistent Effective Medium Theory[40,41] (EMT) to evaluate the effective overall electrical conductivity of this two-phase composite:

$$f = \frac{\sigma_1 - \sigma^*}{\sigma_1 + 2\sigma} + (1-f)\frac{\sigma_2 - \sigma^*}{\sigma_2 + 2\sigma^*} = 0 \quad (1)$$

where $\sigma^*$ is the effective electrical conductivity, $f$ is the volume fraction of pristine grains, $\sigma_1$ and $\sigma_2$ are the electrical conductivities of pristine and doped grains, respectively. Note that the interface scattering between the two phases is ignored in the above equation, and this presumption is reasonable considering the relatively large size (≈500 nm) and the endotaxial crystallographic features of the phase boundaries, as discussed earlier. The individual electrical conductivities ($\sigma = ne\mu$) shall be calculated with the "new" carrier concentrations after charge redistribution and the original carrier mobilities of bulk BiAgSeS and $BiAgSeS_{1-x}Cl_x$.

With the presumption that the total number of charge carriers in pristine and doped grains is conserved during the process of charge transfer and redistribution, at room temperature, the effective electrical conductivity of MD_A is estimated to be ≈14.9 S cm$^{-1}$ and that of MD_B ≈10.7 S cm$^{-1}$ using the model described in SI. In contrast, the experimental values for the two modulation doped samples are 19.9 and 22.8 S cm$^{-1}$ separately. The discrepancy between calculated and experimental results therefore puts doubt on the aforementioned intuitioniztic presumption, and strongly suggests that modulation doping itself is insufficient to explain the experimental electrical conductivities. One possible explanation is that the Cl rich precipitates at the heterogeneous boundaries might serve as electron reserviors, supplying extra electrons to the modulated matrix grains. As seen in Figure 5f,g, the interface between the Cl rich precipitate and the BiAgSeS matrix is endotaxial, which makes charge transfer/diffusion from the precipiates to the matrix highly possible. The mechanism of charge transfer from Cl rich precipitates to matrix grains can be interpreted to be similar to the works of Zhao et al.[33] and Koirala et al.,[34] where nanoscale metallic particles are believed to provide the matrix grain with extra charge carriers. Additional charge transfer from Cl rich precipitates to matrix grains has the same importance as carrier mobility enhancement due to modulation doping, both mechanisms are indispensable to achieve the significantly improved electrical conductivity hence the overall thermoelectric performance.

## 3. Conclusions

In this work, an enhanced thermoelectric figure of merit $ZT \approx 1.23$ was obtained at 773 K in the heterogeneous composite $(BiAgSeS)_{0.5}(BiAgSeS_{0.97}Cl_{0.03})_{0.5}$. This encouraging enhancement on thermoelectric performance over its uniformly doped counterpart $BiAgSeS_{0.985}Cl_{0.015}$ is ascribed to a simultaneous improvement on carrier mobility and concentration. While the improved carrier mobility validates the successful application of modulation doping in bulk BiAgSeS, the surprising enhancement on charge carrier concentration is explained by the extra charge transfer from Cl rich precipitates seated on the phase boundaries between BiAgSeS and $BiAgSeS_{1-x}Cl_x$ grains to the modulated BiAgSeS grains. The heterogeneous composite in this work is to facilitate charge

carrier transport, thus very distinct to the mechanism normally adopted to strengthen interface phonon scattering. Our finding creates new insights and sheds light on further improvements on thermoelectric performance of a wide range of thermoelectric materials simply via constructing heterogeneous composites with proper band alignments.

## 4. Experimental Details

*Synthesis*: Samples with chemical composition $BiAgSeS_{1-x}Cl_x$ ($x$ = 0, 0.03, 0.05) were synthesized by mixing nominal ratios of high purity starting materials of Bi, Ag, Se, S, and $BiCl_3$ in quartz tubes under an $N_2$-filled glove box. The tubes were then evacuated to a pressure of ~$10^{-4}$ Torr, flame-sealed, slowly heated to 723 K in 12 h, then to 1123 K in 4 h, soaked at this temperature for 6 h and subsequently water quenched to room temperature. The obtained ingots were crushed into powders, then ball milled at 250 rpm for 8 h in a planetary ball mill. The obtained powders were densified by spark plasma sintering system (SPS-211Lx, Dr. Sinter, Japan) under the axial compressive stress of 50 MPa in vacuum at 823 K for 6 min, resulting in high dense Ø20 × 7 mm disk-shaped pellets. As for the modulation doped (MD) samples, they were obtained by hand mixing pristine BiAgSeS with $BiAgSeS_{1-x}Cl_x$ ($x$ = 0.03 or 0.05) powders at a preset volume ratio for 10 mins in motar and pestle, followed by the same SPS process; the SPSed samples were then sealed in an evacuated quartz tube with a pressure of ~$10^{-4}$ Torr and annealed at 823 K for 7 days, to ensure that the samples' microstructures are thermodynamically stable at the highest temperature used for the measurements.

*Electrical Transport Properties*: The obtained SPS processed pellets were cut along the radial direction of a disk sample into bars with dimensions about 18 mm × 3 mm × 3 mm that were used for simultaneous measurement of the Seebeck coefficient and the electrical conductivity using an Ulvac Riko ZEM-2 instrument (ZEM-2, ULVAC-RIKO, Japan) under a helium atmosphere from room temperature to 823 K. Heating and cooling cycles gave repeatable electrical properties to verify the thermal stability. Electrical properties obtained from different slices cut from the same pellets were similar, attesting to the homogeneity of the samples. The uncertainty of the Seebeck coefficient and electrical conductivity measurements is 5%. The Hall coefficients, $R_H$, of the samples were measured at room temperature using a physical properties measurement system (PPMS-9T, Quantum Design Inc, USA), a magnetic field of 2 T and electrical current of 30 mA were applied. The carrier concentration ($n_H$) was calculated by $n_H = 1/eR_H$, where e is the electronic charge. The Hall mobility ($\mu$) was calculated by $\mu = \sigma R_H$, where $\sigma$ is the electrical resistivity. The uncertainty of Hall measurement is also 5%.

*Thermal Conductivity*: High density SPS processed pellets were cut along the SPS pressing direction, the thermal and electrical transport properties were measured along the same direction in the sample. The SPS processed pellets were polished into rectangular samples with side length of 6 mm and ≈2 mm thickness for thermal diffusivity measurements. The samples were coated with a thin layer of graphite to minimize errors from the emissivity of the material. The thermal conductivity was calculated from $\kappa = DC_p\rho$, where the thermal diffusivity coefficient ($D$) was measured using the laser flash diffusivity method in a Netzsch LFA427 (NETZSCH, LFA427, Germany), the thermal diffusivity data were analyzed using a Cowan model with pulse correction and heating and cooling cycles give reproducible values for each sample. The specific heat capacity (Cp) was determined by differential scanning calorimetry (NETZSCH DSC 404C Germany). The density ($\rho$) was determined by using the dimensions and mass of the sample, which was then reconfirmed using the Archimedes method. The measured mass density for MD_A and MD_B are 6.610 and 6.731 g/cm$^3$, respectively, which are both around 90% of the theoretical value (7.51 g/cm$^3$), in good agreement with our previous reports.[23] Thermal diffusivities obtained for different slices from the same pellet are also similar. The uncertainty of the thermal conductivity is estimated to be within 8%, considering the uncertainties for $D$, $C_p$, and $\rho$. The combined uncertainty for all measurements involved in the calculation of $ZT$ is less than 14%.

*X-Ray Diffraction and Transmission Electron Microscopy*: Samples pulverized in an agate mortar were used for powder X-ray diffraction, phase structure was analyzed using X-ray diffraction (XRD, CuK$\alpha$, Bruker D8, Germany). Transmission electron microscopy (TEM) investigations were carried out in a FEI Tecnai G2 F20 microscope. The thin TEM specimens were cut from from the exactly same block tested by transport property measurements, and prepared by conventional standard methods, which include cutting, grinding, dimpling, polishing and Ar-ion milling on a liquid nitrogen cooling state subsequently.

## Supporting Information

Supporting Information is available from the Wiley Online Library or from the author.

## Acknowledgements

D.W. and Y.L.P. contributed equally to this work. This contribution was supported by the startup of South University of Science and Technology of China and national 1000 plan for young scientists (J.Q.H.), and partly supported by NSFC under grant No. 51202008 and Postdoctoral Science Foundation of China (2013M540037) (Y.L.P). D. Wu also would like to thank Fengshan Zheng and Xiaoye Liu for their thoughtful discussions and reading on this manuscript.

Received: July 4, 2014
Revised: September 11, 2014
Published online: October 13, 2014

[1] J. P. Heremans, V. Jovovic, E. S. Toberer, A. Saramat, K. Kurosaki, A. Charoenphakdee, S. Yamanaka, G. J. Snyder, *Science* **2008**, *321*, 554.
[2] G. Mahan, J. Sofo, *Proc. Natl. Acad. Sci. U.S.A.* **1996**, *93*, 7436.
[3] W. Liu, X. Tan, K. Yin, H. Liu, X. Tang, J. Shi, Q. Zhang, C. Uher, *Phys. Rev. Lett.* **2012**, *108*, 166601.
[4] Y. Pei, X. Shi, A. LaLonde, H. Wang, L. Chen, G. J. Snyder, *Nature* **2011**, *473*, 66.
[5] G. Zeng, J. M. O. Zide, W. Kim, J. E. Bowers, A. C. Gossard, Z. Bian, Y. Zhang, A. Shakouri, S. L. Singer, A. Majumdar, *J. Appl. Phys.* **2007**, *101*, 034502.
[6] J.-H. Bahk, Z. Bian, A. Shakouri, *Phys. Rev. B* **2013**, *87*, 075204.
[7] H. Liu, X. Shi, F. Xu, L. Zhang, W. Zhang, L. Chen, Q. Li, C. Uher, T. Day, G. J. Snyder, *Nat. Mater.* **2012**, *11*, 422.
[8] C. Xiao, J. Xu, K. Li, J. Feng, J. Yang, Y. Xie, *J. Am. Chem. Soc.* **2012**, *134*, 4287.
[9] K. Biswas, J. He, I. D. Blum, C. I. Wu, T. P. Hogan, D. N. Seidman, V. P. Dravid, M. G. Kanatzidis, *Nature* **2012**, *489*, 414.
[10] L. D. Zhao, V. P. Dravid, M. G. Kanatzidis, *Energ. Environ. Sci.* **2014**, *7*, 251.
[11] J. He, M. G. Kanatzidis, V. P. Dravid, *Mater. Today* **2013**, *16*, 166.
[12] H. Wu, J. Carrete, Z. Zhang, Y. Qu, X. Shen, Z. Wang, L.-D. Zhao, J. He, *NPG Asia Mater.* **2014**, *6*, e108.
[13] H. J. Wu, L. D. Zhao, F. S. Zheng, D. Wu, Y. L. Pei, X. Tong, M. G. Kanatzidis, J. Q. He, *Nat. Commun.* **2014**, *5*, 4515.
[14] B. Sales, D. Mandrus, R. K. Williams, *Science* **1996**, *272*, 1325.
[15] G. S. Nolas, J. Poon, M. Kanatzidis, *MRS Bull.* **2006**, *31*, 199.
[16] S. M. Kauzlarich, S. R. Brown, G. J. Snyder, *Dalton Trans.* **2007**, *21*, 2099.

[17] Y. Wang, N. S. Rogado, R. J. Cava, N. P. Ong, *Nature* **2003**, *423*, 425.
[18] H. Ohta, K. Sugiura, K. Koumoto, *Inorg. Chem.* **2008**, *47*, 8429.
[19] L.-D. Zhao, J. He, D. Berardan, Y. Lin, J.-F. Li, C. Nan, N. Dragoe, *Energy Environ. Sci.* **2014**, *7*, 251.
[20] D. Morelli, V. Jovovic, J. Heremans, *Phys. Rev. Lett.* **2008**, *101*, 035901.
[21] A. Walsh, D. J. Payne, R. G. Egdell, G. W. Watson, *Chem. Soc. Rev.* **2011**, *40*, 4455.
[22] L.-D. Zhao, S.-H. Lo, Y. Zhang, H. Sun, G. Tan, C. Uher, C. Wolverton, V. P. Dravid, M. G. Kanatzidis, *Nature* **2014**, *508*, 373.
[23] Y.-L. Pei, H. Wu, J. Sui, J. Li, D. Berardan, C. Barreteau, L. Pan, N. Dragoe, W.-S. Liu, J. He, L.-D. Zhao, *Energy Environ. Sci.* **2013**, *6*, 1750.
[24] Y. Tung, M. Cohen, *Phys. Rev.* **1969**, *180*, 823.
[25] S. R. Culp, S. J. Poon, N. Hickman, T. M. Tritt, J. Blumm, *Appl. Phys. Lett.* **2006**, *88*, 042106.
[26] G. Joshi, H. Lee, Y. Lan, X. Wang, G. Zhu, D. Wang, R. W. Gould, D. C. Cuff, M. Y. Tang, M. S. Dresselhaus, *Nano Lett.* **2008**, *8*, 4670.
[27] R. Dingle, H. L. Störmer, A. C. Gossard, W. Wiegmann, *Appl. Phys. Lett.* **1978**, *33*, 665.
[28] F. Schäffler, *Semicond. Sci. Technol.* **1997**, *12*, 1515.
[29] R. People, J. C. Bean, D. V. Lang, A. M. Sergent, H. L. Störmer, K. W. Wecht, R. T. Lynch, K. Baldwin, *Appl. Phys. Lett.* **1984**, *45*, 1231.
[30] H. L. Störmer, *Appl. Phys. Lett.* **1981**, *38*, 691.
[31] M. Zebarjadi, G. Joshi, G. Zhu, B. Yu, A. Minnich, Y. Lan, X. Wang, M. Dresselhaus, Z. Ren, G. Chen, *Nano Lett.* **2011**, *11*, 2225.
[32] B. Yu, M. Zebarjadi, H. Wang, K. Lukas, H. Wang, D. Wang, C. Opeil, M. Dresselhaus, G. Chen, Z. Ren, *Nano Lett.* **2012**, *12*, 2077.
[33] H. Zhao, M. Pokharel, S. Chen, B. Liao, K. Lukas, C. Opeil, G. Chen, Z. Ren, *Nanotechnology* **2012**, *23*, 505402.
[34] M. Koirala, H. Zhao, M. Pokharel, S. Chen, T. Dahal, C. Opeil, G. Chen, Z. Ren, *Appl. Phys. Lett.* **2013**, *102*, 213111.
[35] D. J. Bergman, O. Levy, *J. Appl. Phys.* **1991**, *70*, 6821.
[36] Y. Yang, S. H. Xie, F. Y. Ma, J. Y. Li, *J. Appl. Phys.* **2012**, *111*, 013510.
[37] A. J. Minnich, M. S. Dresselhaus, Z. F. Ren, G. Chen, *Energy Environ. Sci.* **2009**, *2*, 466.
[38] K. Biswas, J. He, Q. Zhang, G. Wang, C. Uher, V. P. Dravid, M. G. Kanatzidis, *Nat. Chem.* **2011**, *3*, 160.
[39] A. Mehdizadeh Dehkordi, S. Bhattacharya, T. Darroudi, J. W. Graff, U. Schwingenschlögl, H. N. Alshareef, T. M. Tritt, *Chem. Mater.* **2014**, *26*, 2478.
[40] R. Landauer, *AIP Conf. Proc.* **1978**, *40*, 2.
[41] C.-W. Nan, *Prog. Mater. Sci.* **1993**, *37*, 1.